PCCP
Physical Chemistry Chemical Physics

Accepted Manuscript

This article can be cited before page numbers have been issued, to do this please use: W. Rigaut and F. Calvo, *Phys. Chem. Chem. Phys.*, 2026, DOI: 10.1039/D6CP00043F.

ROYAL SOCIETY OF CHEMISTRY

rsc.li/pccp

View Article Online
DOI: 10.1039/D6CP00043F

Journal Name

ARTICLE TYPE

Cite this: DOI: 00.0000/xxxxxxxxxx

Shape and composition effects on the Debye temperature and breathing frequency of metal nanoparticles†

William Rigaut[a,b] and Florent Calvo[a]

Received Date
Accepted Date

DOI: 00.0000/xxxxxxxxxx

The vibrational properties of metal nanoparticles with dimensions 1–10 nm are computationally explored at the atomistic level of details, without resorting to lattice dynamics in the harmonic approximation. Using molecular dynamics simulations, power spectra of the atomic velocities and a measure of the particle volume are obtained, providing estimates for the vibrational density of states (VDOS) and the breathing frequency, respectively. The Debye temperature is inferred directly from the heat capacity resulting from the VDOS. For monometallic particles made of pure gold or iron, the influence of the shape around the cube reference is scrutinized either by varying the sharpness of their edges, or by varying their anisotropy from flat to elongated particles, keeping the number of atoms as approximately constant. The surface fraction of atoms is found as a leading driving force for the breathing frequency, although it cannot explain alone the more subtle variations of the Debye temperature that rely on the entire VDOS. Bimetallic silver-gold particles are also revisited, focusing on the role of chemical ordering (core-shell versus alloy), composition, and size. While the Debye temperature exhibits relatively modest variations throughout all cases investigated, the breathing frequency shows marked differences upon changes in the shape anisotropy or the chemical ordering, especially in core-shell nanoparticles with 20% composition in the core. Competing breathing modes are often found to arise, especially in weakly deformed iron nanoparticles.

1 Introduction

Metal nanoparticles (NPs) play a key role in nanoscience, owing to their many applications ranging from plasmonics, energy materials, to catalysis and biosciences. Among the various fundamental properties that characterize the behavior of nanoparticles, and besides their structure itself, the vibrations play a particular role as they primarily affect their mechanical stability,[1] dynamics and heat transport,[2] and more generally the response to external (electronic or nuclear) excitations. Inelastic light scattering[3–5] and ultrafast pump-probe spectroscopic[6] techniques are the most direct methods to measure experimentally the vibrational properties of nanoparticles. These methods are often complementary to each other, because they can be sensitive to different vibrational modes. The radial breathing motion, for example, is not expected to be infrared active, while it is one of the main targets of time-resolved or Raman experiments.

The Debye temperature Θ_D is another feature of materials that is intimately tied to their vibrations, through their density of states and the heat capacity derived from it. Besides Raman measurements,[7,8] other techniques based on X-ray spectroscopy such as extended X-ray absorption fine structure[9,10] or nuclear resonant inelastic X-ray scattering,[11] as well as Mössbauer spectroscopy[12,13] have been used to determine the mean-square atomic displacement, which after applying the Debye-Waller formula leads to an estimate of the Debye temperature.

As with any physical or chemical property, it is their size variations caused by the large surface/volume ratio that makes nanoparticles in general, and their vibrational properties in particular, interesting to study. The highly quantized and discrete nature of the vibrations in very small clusters make the use of the continuous models disputable in the first place, an issue which has been specifically discussed for the Debye temperature based on first-principle simulation methods.[14–16] For purely thermodynamic properties, attempts to bridge the gap between small clusters and bulk properties have been suggested,[17] but they contain empirical ingredients and cannot be straightforwardly applied to arbitrary physical or chemical properties.

The convergence of the Debye temperature to the bulk limit is found to be usually monotonic and from below for many metals[7,8,11–13,18] as well as bimetallic NPs,[19] with corrections that scale with the number atoms N (or the radius R for approximately spherical 3D nanoparticles) as $N^{-1/3}$ (or $1/R$). In a few cases,

[a] Université Grenoble Alpes, CNRS, LiPhy, 38000 Grenoble, France
[b] Institut Néel, CNRS, Université Grenoble Alpes, F-38042 Grenoble, France Université Grenoble Alpes, CNRS, LiPhy, 38000 Grenoble, France

† Electronic Supplementary Information (ESI) available: [Number of atoms and prolateness parameters for each set of nanoparticles (Tables S1-S5), as well as detailed geometries of the pure particles as separate files.]. See DOI: 00.0000/00000000.

View Article Online
DOI: 10.1039/D6CP00043F

more complex variations in Θ_D with increasing particle size were reported, either converging to the bulk limit from above [9,10] or remaining below the bulk limit. [11] Such puzzling results were reinvestigated [20] and shown to be possibly caused by the presence of the environment of the nanoparticles, and partly be artifacts. From the theoretical perspective, monotonic size effects with corrections scaling as the inverse radius are often assumed to hold in thermodynamical models, [21–25] but have also been supported by simulations directly at the atomistic level, at least in the case of iron NPs. [26]

For large enough isotropic particles, the size variations of the radial breathing frequency ω_b generally follow Lamb's theory of continuous media, which predicts a simple scaling law $\omega_b(N) \propto N^{-1/3}$. This result is supported by experiments [27] and has been confirmed at the atomistic level. [28,29] Beyond scaling trends, several groups have questioned the validity of continuous elasticity theory for finite metal nanoclusters [28–31] as well as other nanostructures such as fullerenes. [32]

Nanoparticles that are structurally or chemically heterogeneous, exhibitting e.g. deformed shapes or multiple elements, naturally pose a greater challenge to continuous media theories. This issue has been specifically addressed in the past, either by extending such approaches to nonspherical shapes [33,34] or core-shell bimetallic spheres, [4] or by applying harmonic approximations to the radial motion of nanoalloys with various types of chemical orderings. [29] The effects of shape on the breathing modes of metal nanoparticles were addressed by Sauceda and coworkers, [28] who found little differences between decahedral (oblate) particles and more isotropic particles. The acoustic vibrations of strongly elongated (prolate) nanowires have also been experimentally investigated. [35,36]

In the present work, we consider separately the effects of shape, composition, chemical ordering, and size on the Debye temperature and the radial breathing frequency of metal nanoparticles ranging from 150 to 15,000 atoms, that is reaching up to about 7 nm equivalent diameter. Such sizes are larger than previously considered nanostructures in the present context, making explicit electronic structure methods and more generally static approaches based on harmonic approximations very unpractical. Instead we fully account for anharmonicities at finite temperature through molecular dynamics (MD) simulations, and exploit appropriate power spectra of atomic velocities or a geometrical measure of the volume to determine the vibrational density of states and the breathing frequency, [31] respectively.

Two types of shape deformations were considered, using the so-called supercube as the reference motif and interpolating it from cubes to spheres and, beyond spheres, into convex shapes, or by stretching it either way along one main axis to produce prolate or oblate nanostructures. Supercubes have been a popular motif for nanoscale objects, especially regarding how their rounding affects their propensity for self-assembly, [37] and the sharpness of the edges is known to affect the stability of metal nanoparticles to a significant extent. [38] By addressing both face-centered cubic (gold) and body-centered cubic (iron) metals and keeping the nanoparticle size as approximately constant, the specific effects of shape on both Θ_D and ω_b could be determined. Anisotropic deformations into oblate or prolate nanostructures are a more challenging case for the breathing mode, because the assignment of the breathing motion based on volumic variations can be more ambiguous .citelansun Finally, bimetallic nanoparticles of miscible metals (silver and gold) were also investigated, focusing here on the effects of chemical ordering as in our previous work [29] but without relying on the uniform radial and harmonic approximation.

As a general outcome, our simulations predict that shape effects on the Debye temperature amount to about 10% variation and are thus relatively minor for homogeneous nanoparticles, but are more significant on the breathing frequency, especially for anisotropic deformations, and apart from possible competing modes found for iron NPs. The main conclusions from our earlier study on bimetallic nanoalloys [29] are qualitatively recovered for the breathing frequency of core/shell versus alloyed gold-silver particles, with the interface between the two metals and the relative thicknesses of the core and the shell playing important roles. Furthermore, the Debye temperature for these bimetallic nanoparticles exhibits nontrivial variations with composition that point at the limits of applicability of the simple Debye model to represent heat capacity curves.

2 Methods

2.1 Debye temperature and breathing frequency

The Debye temperature Θ_D was determined from the temperature variations of the heat capacity $C_v(T)$. For a metallic system, C_v includes contributions from the phonons and the electrons, the latter being much smaller and varying as T^3 at low temperature. Neglecting it allows rewriting the heat capacity as a function of the vibrational densities of states (VDOS) $g(\omega)$ only as

$$C_v(T) = 3k_B \int_0^{\omega_{max}} \left(\frac{\hbar\omega}{k_B T}\right)^2 \frac{e^{\hbar\omega/k_B T}}{(e^{\hbar\omega/k_B T}-1)^2} g(\omega) d\omega, \qquad (1)$$

where $\hbar$ and ω_{max} denote the reduced Planck constant and the maximum physical frequency of the system, respectively. To evaluate the VDOS, the velocity time autocorrelation function was employed, yielding [39]

$$g(\omega) \propto \int \frac{\langle \mathbf{v}(t)\cdot\mathbf{v}(0)\rangle}{\langle \mathbf{v}(0)^2\rangle} e^{i\omega t} dt, \qquad (2)$$

in which $\langle\cdot\rangle$ denotes an average over initial conditions, and $\mathbf{v}$ the velocity vector over all atomic coordinates. The proportionality coefficient, absent from the previous equation, is determined *a posteriori* by requiring that the VDOS normalizes to the total number of vibrational degrees of freedom of the system,

$$\int g(\omega) d\omega = 3N - 6. \qquad (3)$$

In the Debye model, the VDOS is assumed to have a quadratic form,

$$g_{Debye}(\omega) = \gamma\omega^2 \Theta(\omega_c - \omega), \qquad (4)$$

where γ is a positive constant that depends on the element only, $\Theta(x)$ the Heaviside step function, and ω_c a positive cut-off frequency. This leads to the following expression of the specific heat

View Article Online
DOI: 10.1039/D6CP00043F

in the Debye approximation,

$$C_v^{\text{Debye}}(T) = 9k_{\text{B}}\left(\frac{T}{\Theta_{\text{D}}}\right)^3 \int_0^{\Theta_{\text{D}}/T} \frac{x^4 e^x}{(e^x-1)^2} dx, \tag{5}$$

In this equation, $\Theta_{\text{D}} = \hbar\omega_c/k_{\text{B}}$ defines the Debye temperature.

In practice, given a density of vibrational states $g(\omega)$ determined by molecular dynamics simulations, the temperature variations of the heat capacity are numerically obtained by application of Eq. (1). A Debye temperature Θ_{D} is then inferred by minimizing the least-square error between these variations and those of the corresponding Debye model of Eq. (5).

The breathing frequency ω_{b} is a particular vibrational mode which directly affects the volume of the material. Following Lan and Sun,[31] we identify ω_{b} from its signature of a maximum peak in the power spectrum associated to the volume $\mathscr{V}$ of the nanostructure, which acts as its conjugate variable. Several definitions for the volume of nanoparticles described at the atomistic level of details have been proposed in the past.[31,40] Here we follow the work by Sun and Gong,[41] in which a simple additive expression for $\mathscr{V}$ that takes into account the different local environments of individual atoms, thus the existence of surface versus bulk atoms, was proposed:

$$\mathscr{V} = \sum_i v_i \tag{6}$$

$$v_i = \gamma_i \frac{4\pi}{3} \sum_{j\in\text{n.n.}} \left(\frac{r_{ij}}{2}\right)^3. \tag{7}$$

In the above equations, v_i stands as the volume associated with atom i in its environment with nearest-neighbor (n.n.) atoms j, r_{ij} the distance between them, and γ_i a scaling factor taken here as 1 for all atom types. Nearest neighbors are here defined based on a simple distance criterion, $r_{ij} < 3$ Å.

For small enough nanoparticles, a full harmonic approximation can be conducted to yield not only the vibrational frequencies $\{\omega_k, k = 1\ldots 3N-6\}$, but also the related eigenvectors which we denote as $\{\vec{u}_{i,k}, i = 1\ldots N\}$ for any $k = 1\ldots 3N-6$. The contribution of each of these modes to the radial breathing mode can be quantified by projecting them radially, that is introducing

$$P_k = \sum_i \vec{r}_i \cdot \vec{u}_{i,k} \tag{8}$$

for each mode k, and defining arbitrarily the radial breathing frequency ω_b as the frequency ω_k for which the magnitude of P_k is maximum. In the Supplementary Material, we show that this definition compares well with the anharmonic spectra inferred from MD simulations for small gold and iron nanoparticles, including in the rather common cases of multiple competing peaks and up to expected redshift effects in the anharmonic case.

The full harmonic calculation being unpractical for most system sizes considered in the present work, a simpler approximation was also occasionally considered, in which the breathing frequency is assumed to describe the vibrational response of the system to a *uniform* radial deformation.[29] This approximation may appear particularly stringent for anisotropic nanoparticles, for which the deformation is multiaxial. Within this approach, the breathing frequency reads

$$\omega_{\text{b}} \approx \sqrt{W/I} \tag{9}$$

$$I = \sum_i m_i q_i^2 \tag{10}$$

$$W = \sum_{i,j} q_i q_j \left.\frac{\partial^2 V}{\partial q_i \partial q_j}\right|_0, \tag{11}$$

where $\{q_i\}$ denotes the $3N$ Cartesian coordinates of the system, m_i the corresponding atomic mass, and with the second derivative of the potential in Eq. (11) being taken at the equilibrium geometry. With respect to conventional harmonic approaches, in which the breathing frequency is obtained as the normal mode frequency maximizing the radial component of its individual eigenmode, the above simplified approach does not require the full diagonalization of the mass-weighted Hessian matrix, which for particles exceeding 10,000 atoms is a limiting step.

The value of ω_b obtained using this radial uniform harmonic approximation falls close to a strongly radial harmonic frequency of the system, and is even quantitative in the case of iron nanoparticles (also see the Supplementary Material).

2.2 Structures of Nanoparticles

The nanoparticles are described at the atomistic level of details, assuming prescribed outer shapes and the most natural crystallographic ordering, namely face-centered cubic for gold and body-centered cubic for iron NPs. Two varieties of shapes were considered depending on the system, based on supercubes for both iron and gold NPs.

Supercubes are generally defined by a rounding exponent m, atoms with Cartesian positions x, y, and z being part of the NP if their positions satisfy

$$\left|\frac{x}{a}\right|^m + \left|\frac{y}{b}\right|^m + \left|\frac{z}{c}\right|^m \leq 1, \tag{12}$$

where a, b, and c are the dimensions along the x, y, and z directions, respectively. While a rounding exponent $m = 2$ defines ellipsoidal NPs, large values $m \to \infty$ describe increasingly sharp edges, whereas $m = 1$ describes octahedra, lower values $m < 1$ being ascribed to convex shapes. A first series of isotropic nanoparticles were constructed by fixing m, then truncating a large enough cristallographic sample, keeping only those atoms that fulfill Eq. (12) above, varying $a = b = c$ in such a way to reach approximately 10,000–10,500 atoms. The main geometrical features of the resulting nanoparticles (outer dimensions, numbers of atoms) are given in the Supplementary Material as a function of the rounding exponent m in Tables S2 and S3 for gold and iron nanoparticles, respectively.

To investigate specifically the role of anisotropic deformations, a similar strategy of truncating a large crystallographic sample was pursued. The boundary definition was adjusted to include a central rectangular cuboid with flat facets along the x, y, and z directions, scaling either the z dimension alone to yield elongated (prolate) NPs, or both x and y to yield flattened (oblate) NPs. Outer layers were then added with rounded edges $m = 3$,

View Article Online
DOI: 10.1039/D6CP00043F

as defined above, acting over a thickness of 5 Å. Here again, the dimensions along the three Cartesian axes were varied in order to reach a total number of atoms of approximately 10,000. The resulting deformation was characterized using the dimensionless prolateness parameter P defined from the principal momenta of inertia I_x, I_y and I_z as

$$P = \frac{I_x - I_z}{I_x + I_y + I_z}, \tag{13}$$

in which, by construction and symmetry, $I_x = I_y$. Elongated particles are such that $I_x > I_z$, hence $P > 0$, whereas flattened particles have $P < 0$ and only the isotropic cube has $P = 0$. Tables S4 and S5 in the Supplementary Material provide the main geometrical features of the resulting nanoparticles (outer dimensions along the x, y, and z axes, numbers of atoms) as a function of the prolateness parameter for gold and iron nanoparticles, respectively.

For the bimetallic Ag-Au nanoparticles, multilayer icosahedral shapes were considered, as they are the relevant motif at least for silver NPs[42] and naturally support core-shell arrangements. The size of these NPs is exactly dictated by the number of layers, which varies between 3 and 16, or between 55 and 14,993 atoms, respectively. Perfect core-shell geometries were first constructed by imposing that the inner n layers and outer p layers only contain atoms of a prescribed type, Ag or Au. Due to the increasingly large number of atoms in the successive layers, the relative composition in gold and silver varies stepwise and irregularly with increasing number of layers. The numbers of atoms and outer radii of the pure gold and silver nanoparticles are listed in Table S5 of the Supplementary Material. Besides core-shell geometries, alloyed NPs were also produced, by randomly mixing the silver and gold atoms inside the icosahedral lattice, assuming a fixed Ag-Au composition varying from 0 to 100% by steps of 10%.

2.3 Computational details

Well-established many-body potentials were chosen to model the interactions in the iron, gold, and gold-silver nanoparticles containing up to almost 15,000 atoms. For iron, the Mendelev potential[43] was chosen owing to its good performance for energetic, structural, and vibrational properties of bulk iron in the BCC phase.

For gold, silver, and their mixtures, we resorted to the same second-moment approximation (SMA) model as pioneered by Cleri and Rosato[44] and reparametrized for these elements at the nanoscale by Rossi and coworkers.[45] The very same potential was employed in our earlier study of gold-silver nanoalloys,[29] allowing a direct comparison and assessment of the harmonic uniform radial approximation for the breathing frequency.

For each nanoparticle, the geometry was initially locally minimized using conjugate gradient optimization. Molecular dynamics trajectories were then carried out in the microcanonical ensemble, starting from the minimized geometry and after distributing randomly the velocities and scaling them in order to reach an approximate kinetic temperature of 300 K: this is achieved by giving an initial kinetic energy of 600 K, which after relaxation and energy equipartition amounts to populate the vibrational modes at the requested temperature. This initial velocity distribution was also constrained not to carry any global linear or angular velocity for the entire nanoparticles, keeping the total number of independent degrees of freedom to be $3N-6$, with N being the number of atoms.

The velocity Verlet algorithm was employed to propagate the classical equations of motion under the many-body potential appropriately chosen for each nanoparticle. All trajectories were integrated for 1 ns, using a time step of 1 fs. The time correlation functions for alloyed silver-gold particles were averaged over 10 independent realizations of random chemical disorder. For all pure and core-shell nanoparticles, 10 trajectories were also performed, differing in the assignment of initial velocity vectors, all under the constraint of vanishing linear and angular momenta.

During a simulation, the velocity and volume autocorrelation functions were accumulated over 8192 successions of 4 fs (four time steps) time lapses. After Fourier transformation, this yields a spectral resolution of about 1 cm^{-1}, and a maximum accessible frequency exceeding 4000 cm^{-1}, much above the range of physical frequencies that largely cover the densities of states obtained for all NPs ($\omega < 500$ cm^{-1}).

In larger nanoparticles, the resolution of 1 cm^{-1} appears somewhat too coarse, and to alleviate this numerical issue without resorting to excessively long simulation times, a simple Gaussian broadening of 1 cm^{-1} was applied to the raw spectrum but on a finer grid of 0.1 cm^{-1}. The breathing frequency was numerically determined from the maximum of this convoluted spectrum.

Except for highly convex particles with low rounding exponents, all particles were found to be stable at 300 K. At this temperature, the protruding nature of the particles with $m < 0.5$ (gold) and $m < 0.75$ (iron) made them rearrange into more compact shapes, with m increasing significantly closer to 1, thereby putting lower limits for the range of the rounding exponent considered for the two metals.

3 Shape effects: monometallic particles

Monometallic nanoparticles were constructed by retrieving from a large cristallographic sample the atoms inside a generic three-dimensional surface defined by Cartesian coordinates along the three x, y, and z orthogonal dimensions. Isotropic shapes belonging to the family of supercubes and covering convex, spherical, and concave nanoparticles with increasingly sharp edges are defined from the single parameter m that is referred to as the rounding exponent. For any value of m, appropriate scaling of the boundary of this outer surface is achieved in order to reach a nanoparticle size of approximately 10,000–10,500 atoms. In addition, elongated and flattened particles were constructed around the cubic motif with rounded edges by stretching the boundary along either a single dimension (z), or the other two dimensions (x and y), scaling the outer surface by an appropriate factor and adding rounded extra layers of 5 Å thickness to produce nanoparticles of about 10,000 atoms. More details can be founds in the Methods section, together with the many-body potentials chosen to describe the atomic interactions.

View Article Online
DOI: 10.1039/D6CP00043F

3.1 Gold nanoparticles

The effects of deforming isotropically the nanoparticles from convex to spherical, then to cubic shapes is considered first in the case of gold, for which the cristallographic template is face-centered cubic. Fig. 1(a) shows the variations of the Debye temperature inferred from the vibrational density of states, itself determined by molecular dynamics simulations at room temperature, as a function of increasing rounding parameter m between 0.5 and 10. The most remarkable result here is that Θ_D is almost maximum for the spherical shape, reaching its lowest values for the extrema of the rounding exponent. However, the range of these variations remains relatively moderate and amounts to a few percents only.

Typical densities, represented as an inset for selected values of $m = 0.5$, 2, and 10, display very similar behavior, with one main broad bump peaked near 70 cm^{-1} and a narrower band centered above 100 cm^{-1}. Upon transforming the particle from its most convex shape to the sphere, then to cubes with increasingly sharp edges, it is the intensity of the higher energy peak that varies the most and in a non-monotonic way. This explains why the resulting Debye temperature reaches its maximum near the spherical shapes, but is also consistent with the rather weak amplitude of these overall variations due to the shape, under fixed nanoparticle size.

The corresponding variations of the breathing frequency with increasing rounding exponent are shown in Fig. 1(b). Here the variations in ω_b due to the shape are stronger in magnitude than for the Debye temperature and reach about 20%, but only for strongly convex particles: when m varies between 1 and 10, or for particles evolving from the octahedral to the perfect cubic shapes, the breathing frequency exhibits a rather constant value. This feature is visible on the three power spectra of the volume, for $m = 0.75$, 3, and 10, shown as an inset in Fig. 1(b), although other spurious lower intensity peaks are clearly visible on these spectra.

The predictions from the simple harmonic approximation assuming uniform radial motion, superimposed in Fig. 1(b), appear rather poor from a pure quantitative footing, even though the relative variations are well reproduced, up to a 8 cm^{-1} shift, if the convex region is omitted from the analysis. Such a similarity is supported by comparable residual size effects that can be perceived on the local extrema found for $m = 1.5$ and $m = 3.5$, and that we interpret as being due to the slightly larger or lower numbers of atoms in these nanoparticles (see Table S2 in the Supplementary Material). These results are consistent with the recent study by Saviot[34] based on continuous elasticity theory, who found that the effects of edge rounding were stronger on the convex side of the structural diagram.

The Debye temperature and breathing frequency of prolate or oblate gold nanoparticles containing approximately 10,000 atoms are depicted in Figs. 2(a) and 2(b) as increasing functions of the prolateness parameter P. Such deformations only marginally impact the Debye temperature and vibrational densities of states (not shown), the intrinsic fluctuations due to size variations across the P series being of comparable magnitude (a fraction of Kelvin) as those due to the shape itself. A trend was

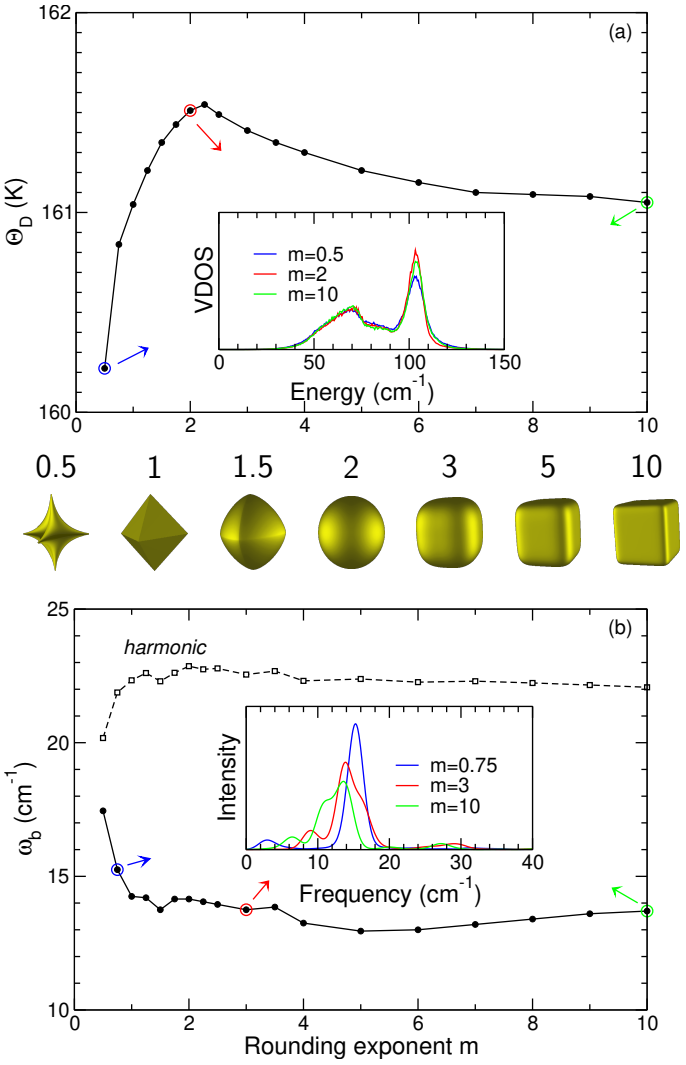

Fig. 1 (a) Debye temperature Θ_D of gold nanoparticles as a function of the rounding exponent m. The inset shows the vibrational densities of states obtained at three values of m; (b) Corresponding variations of the breathing frequency ω_b inferred from molecular dynamics trajectories (solid circles), or the harmonic approximation assuming a uniform radial deformation (empty squares). The inset shows the power spectra of the volume at three values of the rounding exponent. The shapes of the nanoparticles for m =0.5, 1, 1.5, 2, 3, 5, and 10 are depicted between the two panels.

View Article Online
DOI: 10.1039/D6CP00043F

numerically extracted by fitting the data to a cubic polynomial, suggesting that both prolate and oblate deformations tend to decrease Θ_D. In contrast, the effects on the breathing frequency are more significant, especially considering that ω_b reaches its lowest value in the isotropic cubic limit $P = 0$. As the nanoparticle flattens, ω_b increases up to almost 70%, and even doubles in the most extreme elongated case. Here again, the harmonic approximation on the uniform radial motion fails quite spectacularly, predicting opposite trends for the breathing frequency with respect to the fully anharmonic calculation based on molecular dynamics.

These results are consistent with the earlier conclusions by Sauceda and coworkers,[28] in which moderately deformed nanoparticles (decahedral with $P \simeq -0.05$) were considered, but indicate that much stronger effects are to be anticipated in extremely deformed nanoparticles.

To some extent, the variations found for the breathing frequency correlate with the surface fractions of atoms, shown as Supplementary Material in Fig. S2 for both types of deformations, thus confirming the greater importance of surface atoms for this property. However, such a conclusion does not immediately extend to the Debye temperature, this property being sensitive to the entire set of vibrational modes.

3.2 Iron nanoparticles

Iron nanoparticles of 10,000–10,500 atoms were constructed following the same computational procedure as with gold NPs, but using the body-centered cubic crystal as the underlying template. The variations of Θ_D and ω_b with increasing rounding exponent m are represented in Fig. 3(a) and 3(b), respectively. Varying the shape of the iron nanoparticles from convex to octahedral, spherical, and cubic shape with increasingly sharp edges leads to a Debye temperature that also varies only by relatively moderate amounts of less than 2%, with a maximum near $m = 1.5$ and an essentially flat behavior once the concave regime is reached. Typical vibrational densities of states superimposed in the inset of Fig. 3(a) show that it is a redshift of the high-frequency peak near 260 cm^{-1} that is causing the drop in Θ_D in convex particles $m < 1$, the overall VDOS remaining almost constant in the concave region $m \geq 2$.

As was the case with gold nanoparticles, the breathing frequency shows a more sensitive dependence on the rounding parameter, also non-monotonic but with values in the most convex system ($m = 0.75$) and in the sharpest cubic particles ($m > 6$) that deviate from the generic behavior in the intermediate regime. Note that, for this metal, it was not possible to produce stable nanoparticles containing about 10,000 atoms based on the bcc lattice and with even more convex shapes having $m = 0.5$. Three power spectra from which these values of ω_b were determined are depicted in the inset of Fig. 3(b). They all exhibit two peaks, which for $m > 2$ are close to one another near 25 cm^{-1} and 30 cm^{-1}, and the abrupt change in ω_b when m reaches 7 results from the variations in the relative intensities of these two peaks. For these iron nanoparticles, the disagreement between the harmonic and anharmonic breathing frequencies cannot be explained by a mere global shift, although it is noteworthy that

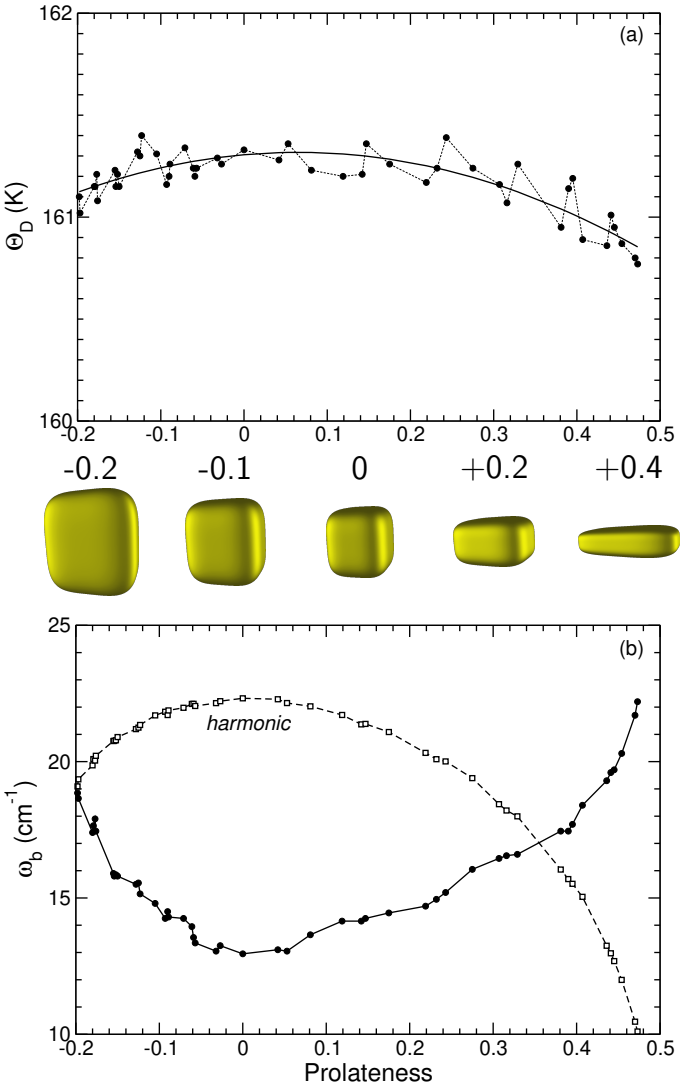

Fig. 2 (a) Debye temperature Θ_D of anisotropic gold nanoparticles, as a function of their prolateness P (black circles), adjusted using a cubic polynomial (solid line); (b) Corresponding variations of the breathing frequency ω_b inferred from molecular dynamics trajectories (black circles) or the harmonic approximation assuming a uniform radial deformation (empty squares). Schematized pictures of the deformed particles for selected values of the prolateness parameter $P = -0.2$, -0.1, 0, 0.2, and 0.4 are depicted between the two panels.

View Article Online
DOI: 10.1039/D6CP00043F

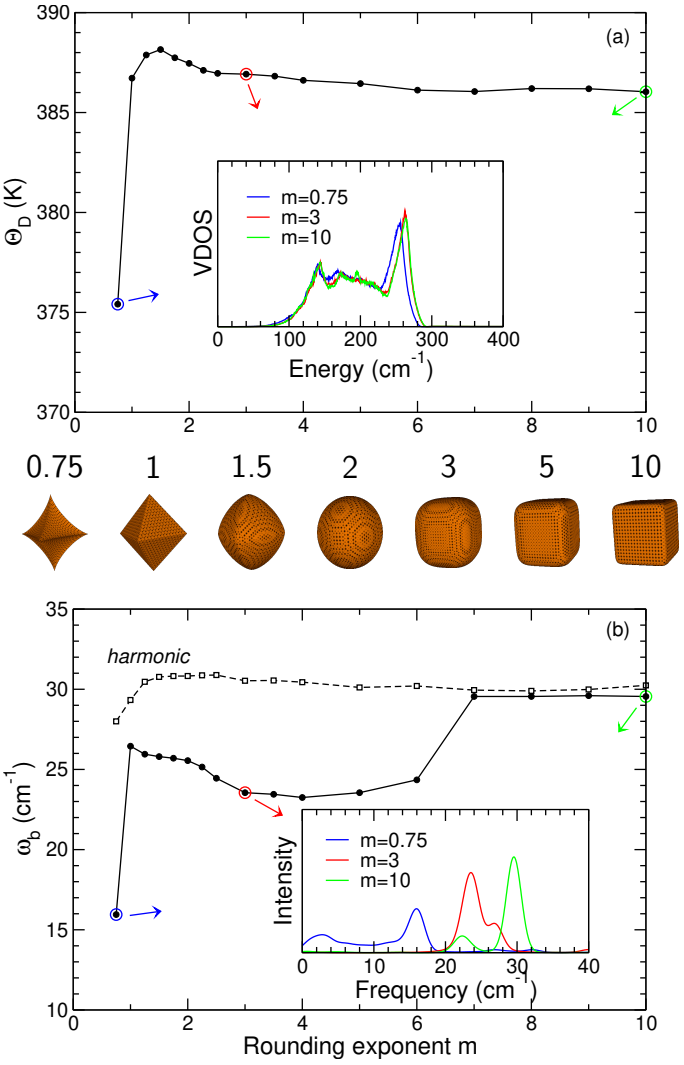

Fig. 3 (a) Debye temperature Θ_D of iron nanoparticles as a function of the rounding exponent m. The inset shows the vibrational densities of states obtained at three values of m; (b) Corresponding variations of the breathing frequency ω_b inferred from molecular dynamics trajectories (solid circles), or the harmonic approximation assuming a uniform radial deformation (empty squares). The inset shows the power spectra of the volume at three values of the rounding exponent. The shapes of the nanoparticles for m =0.75, 1, 1.5, 2, 3, 5, and 10 are depicted between the two panels.

the harmonic approximation performs almost quantitatively for sharp cubes.

The effects of an oblate-to-prolate deformation around the cubic reference on the vibrational properties are illustrated in Fig. 4. Similar to gold, the Debye temperature depicted in Fig. 4(a) exhibits a maximum near the isotropic shape, with relatively smooth variations that are well captured by the cubic polynomial and residual particle size effects. The magnitude of these variations remains moderate, and again below 2% in the entire range of the prolateness parameter. The breathing frequency was more difficult to determine, due to the competition between multiple peaks in the volume power spectrum, as previously discussed in relation with Fig. 3(b) and also illustrated in Fig. S1(a) of the Supplementary Material for the small Au_{147} icosahedral nanoparticle. This competition is clearly evidenced on the three power spectra obtained for $P = 0.043$, 0, and 0.103, shown in the inset of Fig. 4(b). For fairness, two values for ω_b are thus provided in Fig. 4(b) in the prolateness range where this competition is most prominent, namely $-0.104 \leq P \leq 0.136$. The upper branch is more closely connected to the single peak found away from the competing range, and shows overall variations with increasing prolateness that are comparable to the corresponding results found for similarly deformed gold NPs in Fig. 2(b). The same conclusion is reached for the harmonic prediction based on the assumption of uniform radial breathing motion, which again qualitatively fails in reproducing the variations in ω_b due to shape deformations.

The existence of multiple peaks associated with the power spectra of volume indicators, which was discussed at length by Lan and Sun,[31] is a manifestation of anisotropic nanostructures having their volume varying upon the activation of several vibrational modes. Comparison between the two types of metallic particles further indicates that the most intense peak, i.e. the one leading to the largest volume variations, may be appropriate for some metals, but more ambiguous for others.

Finally, it is interesting to note that, as was the case for gold NPs, there is some correlation between the surface ratio and the breathing frequency, at least for moderate values of the rounding exponent (see Fig. S2 of the Supplementary Material) and, albeit to a lower extent with the Debye temperature as well.

4 Compositional and size effects: silver-gold nanoalloys

The Debye temperature and breathing frequency of silver-gold nanoalloys is next considered, examining first the effects of varying their composition. Here we have selected icosahedral nanoparticles with 14 layers and amounting to approximately 10,000 atoms (see Table S5 in the Supplementary Material). Figs. 5(a) and 5(b) show the variations of Θ_D and ω_b for increasing concentration in silver, for core-shell particles of the $Ag_{core}Au_{shell}$ (Ag@Au) and $Au_{core}Ag_{shell}$ (Au@Ag) types, as well as randomly alloyed Ag-Au particles. The choice of the 14-layer icosahedron was also made as it allows almost perfect equicomposition to be reached for the core-shell systems with 11 inner shells of one metal (5083 atoms) and the three outer shells of the other metal (5096 atoms). Nonlinear effects are surprisingly

View Article Online
DOI: 10.1039/D6CP00043F

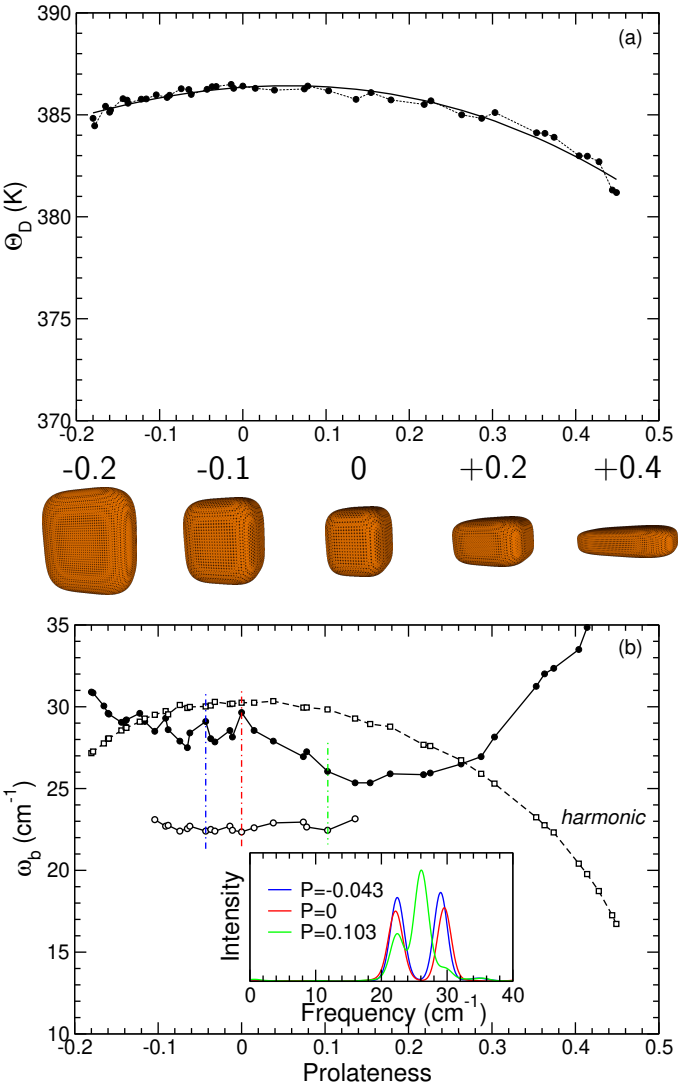

Fig. 4 (a) Debye temperature Θ_D of anisotropic iron nanoparticles, as a function of their prolateness parameter P (black circles), adjusted using a cubic polynomial (solid line); (b) Corresponding variations of the breathing frequency ω_b inferred from molecular dynamics trajectories (black and empty circles) or the harmonic approximation assuming a uniform radial deformation (empty squares). The inset shows three power spectra of the volume at selected values of P, highlighting the presence of two competing vibrational modes involved in the breathing motion. Schematized pictures of the deformed particles for selected values of the prolateness parameter $P = -0.2$, -0.1, 0, 0.2, and 0.4 are depicted between the two panels.

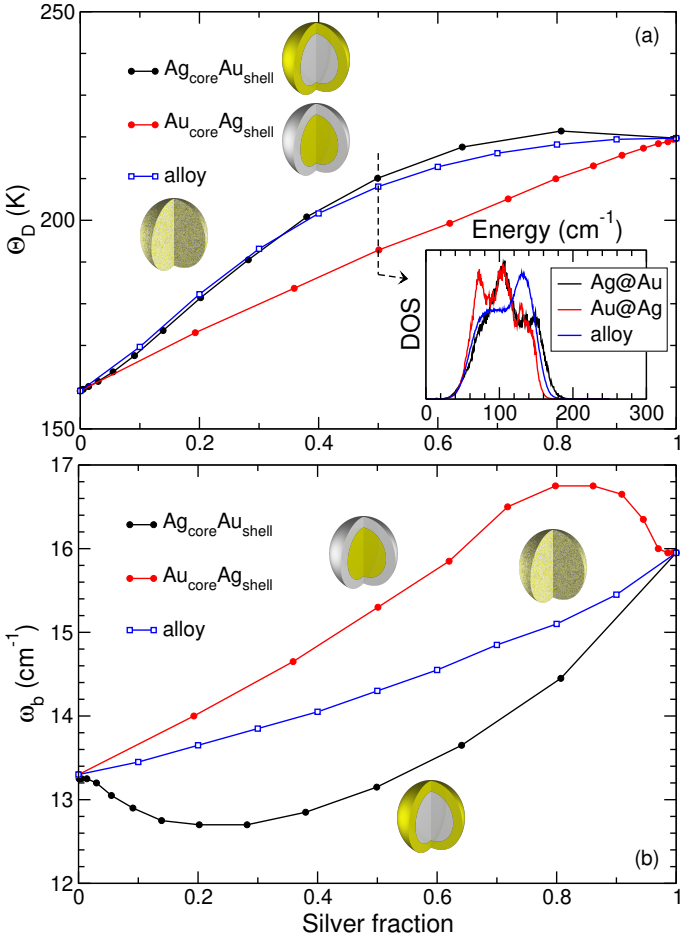

Fig. 5 (a) Debye temperature Θ_D of icosahedral 10179-atom Ag-Au nanoparticles, as an increasing fraction of the silver content and for core/shell particles with either metal in the core, or for randomly alloyed particles. The inset shows the vibrational densities of states of the $Ag_{core}Au_{shell}$ (Ag@Au), $Au_{core}Ag_{shell}$ (Au@Ag), and randomly alloyed Au-Ag particles at 50% composition; (b) Corresponding variations of the breathing frequency ω_b inferred from molecular dynamics trajectories.

View Article Online
DOI: 10.1039/D6CP00043F

strong for the alloyed system, with a clear enhancement in the Debye temperature at intermediate compositions. This effect is even stronger in the Ag@Au NPs, where Θ_D exceeds that of pure silver NPs when doped with 10% gold. Only does the Au@Ag system exhibit mostly linear variations as the silver concentration is increased.

To interpret these rather puzzling results, some vibrational densities of states are shown in the inset of Fig. 5(a) near equiconcentration in the two metals. While the Au@Ag and Ag@Au systems share one main peak near 100 cm^{-1}, they are respectively associated with additional broad bands at lower (80 cm^{-1} for Au@Ag) or higher (120 cm^{-1} for Ag@Au) frequencies. In contrast, the alloyed NPs only display one broad band near 120 cm^{-1} and a shoulder at 80 cm^{-1}. Despite being qualitatively different, the VDOS functions for the alloyed and Ag@Au core-shell NPs give rise to very similar anharmonic heat capacities, hence almost identical Debye temperatures. The lower value of Θ_D in the Au@Ag particle is consistent with the low-frequency peak near 80 cm^{-1} and the absence of any particular feature at higher frequencies.

The breathing frequency of the alloyed particles exhibits rather smooth and weakly nonlinear behavior with varying composition, in agreement with our earlier conclusions based on the harmonic approximation for uniform radial motion.[29] However, the Ag@Au and Au@Ag core-shell particles both undergo strong non-monotonic variations, with absolute minimum and maximum, respectively, occuring when the core concentration approaches 20% in both cases. The deviation to the average value associated with the alloyed particles reference was also noted in the harmonic approach[29] but is found here to be significantly magnified with the present, anharmonic definition of ω_b.

Except in the limit of single metals, all core-shell particles of a given type have the same surface structure and the same size, but differ in the interactions between the different metals. It is instructive to consider the fraction of heterobonds as a possible descriptor of chemical mixing in the system, and Fig. S3 in the Supplementary Material shows the variations of this quantity with increasing silver composition for the three types of chemical ordering. Naturally this fraction is the highest in the alloyed particles at 50% silver. In core-shell particles, it is maximum when the outer shell is made of a single layer. However, these extrema do not correlate with extrema in the breathing frequency, nor can they explain, alone, the counterintuitive variations of the Debye temperature.

Finally, we consider scaling size effects on both vibrational properties in Fig. 6, restricting our discussion to pure nanoparticles of either gold or silver metals, as well as the fully alloyed particles near equicomposition. The case of core-shell particles was not treated any further, owing to the frequent impossibility to reach equicomposition from perfect shell filling combinations (except, and as aforementioned, for the 14-shell system). Both Θ_D and ω_b show variations with increasing number of atoms N that can be approximately represented as linear functions of the inverse radius, $A(N) \approx A(\infty) - \alpha/N^{1/3}$. Ignoring the values for the two smallest nanoparticles ($N \leq 147$) leads to the extrapolated values for the Debye temperature that deviate from the experi-

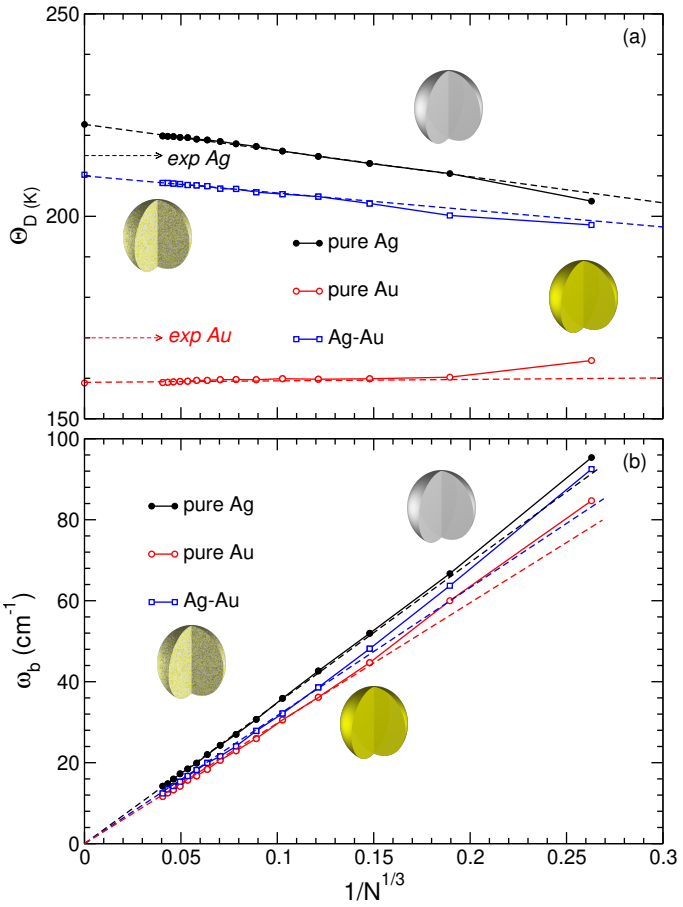

Fig. 6 (a) Debye temperature Θ_D of icosahedral Ag-Au nanoparticles of the core/shell or randomly alloyed types, as a function of their inverse radius $1/N^{1/3}$. The experimentally measured temperatures for the bulk metals are indicated by arrows; (b) Corresponding variations of the breathing frequency ω_b inferred from molecular dynamics trajectories. Dashed lines emphasize the extrapolation, from all nanoparticles but the two smallest ones, to the bulk limiting values $N \to \infty$.

View Article Online
DOI: 10.1039/D6CP00043F

mental data from above for silver (by 8 K) and from below for gold (by 8 K as well). It is noteworthy that, for iron particles, this extrapolation procedure works quantitatively well,[26] which points at intrinsic deficiencies in the potentials used for the noble metals. However, it should also be kept in mind here that the icosahedral lattices on which the properties were calculated are not periodic and do not extrapolate to the true face-centered cubic lattice of the corresponding bulk metals, unlike other cluster shapes based e.g. on the truncated octahedral motif. Yet, the overestimation of Θ_D in finite nanoparticles and relative to the bulk limit is at variance with measurements of this property in thin gold films,[46] and in this respect it would be worth repeating the present simulations under such periodic conditions.

The Ag-Au alloy NPs at equicomposition show Debye temperatures that are significantly closer to those of the pure silver NPs. This result was already noticed in Fig. 5(a) for the specific 10179-atom system, and can be interpreted as the consequence of the strongly nonlinear behavior found for the Debye temperature of alloyed nanoparticles with increasing silver composition. Interestingly, such effects are also much stronger in magnitude than the deviation of the crystal lattice parameter to Vegard's heuristic law for this alloy.[47]

The breathing frequencies naturally scale with the number of atoms as $1/N^{1/3}$, in accordance with Lamb theory for perfect spheres: $\omega_b(N \to \infty) = 0$. This behavior is well reproduced for nanoparticles containing more than 500 atoms, and the scaling factor α depends only marginally on composition: we find $\alpha = 298$ cm^{-1} for pure gold NPs, $\alpha = 347$ cm^{-1} for pure silver NPs, and $\alpha = 316$ cm^{-1} for randomly mixed Ag-Au NPs. These values compare satisfactorily with the predictions from Lamb theory for the pure metals, based on the knowledge of the experimental longitudinal sound velocities and Wigner-Seitz radii,[48] which predict $\alpha(\mathrm{Au}) = 319$ cm^{-1} and $\alpha(\mathrm{Ag}) = 340$ cm^{-1}, given once again the structural deviation between the present icosahedral NPs and the ideal spherical shape.

From Fig. 1 it is tempting to conclude that introducing edges and vertices to the gold nanoparticles (either by transforming them into a cube or into an octahedron) only increases their breathing frequency by a small fraction. Extending this idea to the highly symmetric case of icosahedral particles suggests that the extrapolated scaling factors are upper limits to the ideal spherical case, improving the agreement for silver, but deteriorating it for gold. It seems instead safer to assume that the residual disagreement obtained between the extrapolated scaling factor and the predictions of the Lamb model for perfectly spherical particles based on experimental inputs mainly originates from the intrinsic inaccuracies of the many-body potential used to model the metal nanoparticles. This conclusion is supported by the similar deviations between the Debye temperatures extrapolated from the finite nanoparticles and the bulk experimental limits, which according to Fig. 6(a) indicate a small overestimation for silver, but an equally small underestimation for gold.

5 Conclusion

The influence of the shape of metal nanoparticles on their vibrational properties has long been recognized from spectroscopic experiments,[35,36] as well as dedicated calculations.[31,33,34] Here we have pursued an atomistic approach in which gold and iron particles are modeled by truncating large bulk samples so their outer shape match appropriate supercubes with desired rounding exponents, or elongated or flattened rectangular shapes with varying prolateness. For both gold and iron metals, the Debye temperature Θ_D approaches a maximum for spherical particles, decreasing smoothly as the particle develop edges towards the sharp cubic limit, and more strong strongly as it transforms towards octahedra, then convex supercubes, although the magnitude of such shape effects remains limited to a few percents.

The breathing frequency also remains rather poorly sensitive to shape deformations, except in the limit of strongly convex particles, as well as sharp cubes in the case of iron NPs. However, shape effects are more pronounced and easily exceed 10% relative to the spherical reference, for both gold and iron NPs.

Flattening or elongating the particles around the isotropic cubic shape has a very limited influence on their Debye temperature, which is comparable in magnitude to the intrinsic fluctuations due to size variations, and only shows a weak maximum near the isotropic limit. However, their breathing frequency displays a clear dependence with increasing prolateness that mirrors that of the Debye temperature, but with a much larger magnitude, with ω_b increasing by more than 50% in flat NPs or in long nanowires in the case of gold. A similar behavior is found for iron NPs, although two breathing modes are found to compete with distinct spectral signatures in the case of moderate deformations around the isotropic cube. These variations were found to correlate with the surface atomic fraction.

The case of gold-silver bimetallic nanoparticles was also considered, focusing separately on the effects of chemical ordering, composition and size. A nontrivial enhancement of Θ_D in alloyed particles was found, together with a clearly assymetric role played by the two metals under core/shell configurations, as the result of varying patterns in the underlying densities of vibrational states. In contrast, and while alloyed NPs essentially display a breathing frequency that scales almost linearly with composition, strong nonlinear effects are found in the core/shell configuration, the deviation to the alloy reference being the highest for 20% gold in the core and the lowest near 20% silver in the core. It would definitely be valuable to assess the robustness of these "magic" compositions on other bimetallic systems and shapes other than the icosahedron.

Extrapolating the results obtained for various nanoparticles in the range between 150 and 15,000 atoms, both Debye temperature and breathing frequency vary linearly with inverse particle radius. Such scaling relations confirm the validity of phenomenological macroscopic theories,[21–24] but residual discrepancies with the known experimental limits point at the approximate character of the many-body potentials used to model the bimetallic nanoalloys, but also the pure metals in the first place.

Improving these semi-empirical potentials thus appears as a priority for the present methods to deliver a more quantitative description of vibrational behavior of the noble metal nanoparticles. Most of the current development in interaction potentials for metals relies on machine learning approaches, and usually aims

View Article Online
DOI: 10.1039/D6CP00043F

at developing surrogate models for reference data (energies and forces) obtained with explicit electronic structure methods such as density-functional theory (DFT). The drawback of this strategy is that the vibrational properties are not directly included in the fitting process, except, at best, the elastic constants, and DFT itself is not guaranteed to reproduce experimental data accurately, owing to the known dependence to the details of such calculations, namely functional and basis set. While DFT is obviously preferable to any parametrized method and effectively relevant for small systems,[14–16] it is not suitable for particles approaching the continuum limit and at finite temperatures. In this respect, traditional many-body potentials with their far fewer parameters to be optimized but a fully explicit functional form can more easily aim at reproducing a greater variety of properties, including those such as elastic constants that are the key to vibrational structure. The much better performance of the potential used for bcc iron in reproducing the bulk limit of the Debye temperature by extrapolating nanoparticle data[26] nicely illustrates why this traditional approach remains useful for the present applications, although of course this does not guarantee that the potential remains accurate at the nanoscale, especially given that, ultimately, it is always up to experimental measurements to qualify the computational methodology.

Besides the quality of the underlying potential, the methodology for determining both Θ_D and ω_b based on the power spectra of appropriate properties has its own practical limitations, especially for large nanoparticles. Not only does the computational cost of handling N-atom systems scale at least linearly with N, the scaling of the breathing frequency roughly as $1/N^{1/3}$ requires in principle that the MD simulations should become increasingly long and themselve scale as $N^{1/3}$, in order to keep a spectral resolution approximately constant when applying the Fourier transform. This issue, which is even worse for the acoustic gap (or lowest vibrational frequency), would make it difficult to reliably treat systems exceeding about 10 nanometers in all three dimensions.

Finally, and as already discussed by Lan and Sun,[31] the possible presence of multiple spectral signatures of the breathing motion that was reported here notably for cubic iron particles may require monitoring other, alternative observables that are sensitive to the volume. The convex hull, for instance, provides a natural connection with the notion of embedding surface that makes it also more related to continuum approaches.[40]

Once these aspects are clarified, it could be useful to extend the methodology further to address more realistic nanoparticles not necessarily in the gas phase. Environmental effects, either surfactants and a liquid for chemically synthesized colloidal particles or a matrix or a solid substrate for physically synthesized particles, are essential in all practical applications of nanoscience and of course change their vibrational properties. Moreover, altering the shape of nanoparticles is precisely achieved by varying the surfactants themselves, among other experimental conditions. Although they require dedicated modeling, environmental effects can be straightforwardly taken into account, still using appropriate power spectra in molecular dynamics simulations.

Conflicts of interest

There are no conflicts to declare.

Author contributions

William Rigaut: Conceptualization (supporting); Formal analysis (equal); Investigation (equal); Methodology (supporting); Software (supporting); Writing - Original draft preparation (supporting) **Florent Calvo:** Conceptualization (lead); Formal analysis (equal); Investigation (equal); Methodology (lead); Software (lead); Writing - Original draft preparation (lead)

Acknowledgements

Some of the results presented in this work were obtained on the computing center Pôle Scientifique de la Modélisation Numérique (PSMN) in Lyon, which we gratefully acknowledge.

Notes and references

1 W. Heni, L. Vonna and H. Haidara, *Nano Lett.*, 2015, **15**, 442.
2 A. Alkudi, J. Lombard, F. Detcheverry and S. Merabia, *Phys. Rev. Appl.*, 2020, **13**, 034036.
3 L. Saviot, C. H. Netting, D. B. Murray, S. Rols, A. Mermet, A.-L. Papa, C. Pighini, D. Aymes and N. Millot, *Phys. Rev. B*, 2008, **78**, 245426.
4 H. Portales, L. Saviot, E. Duval, M. Gaudry, E. Cottancin, M. Pellarin, J. Lermé and M. Broyer, *Phys. Rev. B*, 2002, **65**, 165422.
5 D. Ristić, M. Ivanda, K. Furić, U. V. Desnica, M. Buljan, M. Montagna, M. Ferrari, A. Chiasera and Y. J. Jestin, *J. Appl. Phys.*, 2008, **104**, 073519.
6 A. Crut, P. Maioli, N. D. Fatti and F. Vallée, *Phys. Rep.*, 2018, **549**, 1–43.
7 M. Bayle, N. Combe, N. M. Sangeetha, G. Viau and R. Carles, *Nanoscale*, 2014, **6**, 9157.
8 R. Carles, P. Benzo, B. Pécassou and C. Bonafos, *Sci. Rep.*, 2016, **6**, 39164.
9 S. I. Sanchez, L. D. Menard, A. Bram, J. H. Kang, M. W. Small, R. G. Nuzzo and A. I. Frenkel, *J. Am. Chem. Soc.*, 2009, **131**, 7040.
10 B. R. Cuenya, M. A. Ortigoza, L. K. Ono, F. Behafarid, S. Mostafa, J. R. Croy, K. Paredis, G. Shafai, T. S. Rahman, L. Li, Z. Zhang and J. C. Yang, *Phys. Rev. B*, 2011, **84**, 245438.
11 B. R. Cuenya, L. K. Ono, J. R. Croy, K. Paredis, A. Kara, H. Heinrich, J. Zhao, E. E. Alp, A. T. DelaRiva, A. Datye, E. A. Stach and W. Keune, *Phys. Rev. B*, 2012, **86**, 165406.
12 M. Hou, M. E. Azzaoui, H. Pattyn, J. Verheyden, G. Koops and G. Zhang, *Phys. Rev. B*, 2000, **62**, 5117.
13 U. Herr, J. Jing, B. Birringer, U. Gonser and H. Gleiter., *Appl. Phys. Lett.*, 1987, **50**, 472.
14 G. Shafai, M. A. Ortigoza and T. S. Rahman, *J. Phys.: Cond. Matt.*, 2012, **24**, 104026.
15 H. E. Sauceda, F. Salazar, L. A. Pérez and I. L. Garzón, *J. Phys. Chem. C*, 2013, **117**, 25160.
16 A. S. Maldonado, R. Faccio and S. B. Ramos, *J. Mol. Graph. Model.*, 2023, **121**, 108445.

View Article Online
DOI: 10.1039/D6CP00043F

17 A. V. P. B. I. Loukhovitski and A. S. Sharipov, *Phys. Chem. Chem. Phys.*, 2022, **24**, 13130–13148.
18 A. Balerna, E. Bernieri, P. Picozzi, A. Reale, S. Santucci, E. Burattini and S. Mobilio, *Phys. Rev. B*, 1985, **31**, 5058.
19 U. Herr, M. Geigl and K. Samwer, *Philos. Mag. A*, 1998, **77**, 641.
20 J. Timoshenko, M. Ahmadi and B. R. Cuenya, *J. Phys. Chem. C*, 2019, **123**, 20594.
21 C. C. Yang, M. X. Xiao, W. Li and Q. Jiang, *Solid State Commun.*, 2006, **139**, 148.
22 C. C. Yang and S. Li, *Phys. Status Solidi B*, 2011, **248**, 1375.
23 K. Sadaiyandi, *Mater. Chem. Phys.*, 2009, **115**, 703.
24 G. Ouyang, Z. M. Zhu, W. G. Zhu and C. Q. Sun, *J. Phys. Chem. C*, 2010, **114**, 1805.
25 X. Jiang, H. Sheng and B. Xiao, *Phys. Chem. Chem. Phys.*, 2023, **25**, 29310–29314.
26 T. Vasina, F. Calvo, J. Bernard and M. Benoit, *Phys. Rev. B*, 2022, **105**, 005400.
27 H. K. Yadav, V. Gupta, K. Sreenivas, S. P. Singh, B. Sundarakannan and R. S. Katiyar, *Phys. Rev. Lett.*, 2006, **97**, 085502.
28 H. E. Sauceda, D. Mongin, P. Maioli, A. Crut, M. Pellarin, N. D. Fatti, F. Vallée and I. L. Garzón, *J. Phys. Chem. C*, 2012, **116**, 25147.
29 F. Calvo, *J. Phys. Chem. C*, 2011, **115**, 17730.
30 N. Combe and L. Saviot, *Phys. Rev. B*, 2009, **80**, 035411.
31 B. Lan and D. Y. Sun, *Phys. Rev. B*, 2021, **103**, 134108.
32 J. N. Petroza-Montero, I. L. Garzón and H. E. Sauceda, *Eur. Phys. J. D*, 2022, **76**, 123.
33 L. Saviot and D. B. Murray, *Phys. Rev. B*, 2009, **79**, 214101.
34 L. Saviot, *Nanomaterials*, 2021, **11**, 1838.
35 W. M. Visscher, A. Migliori, T. M. Bell and R. A. Reinert, *J. Acoust. Soc. Am.*, 1991, **90**, 2154.
36 S. V. Goupalov, *Nano Lett.*, 2014, **14**, 1590.
37 R. Ni, A. P. Gantapara, J. de Graaf, R. van Roij and M. Dijkstra, *Soft Matter*, 2012, **8**, 8826.
38 D. Alpay, L. Peng and L. D. Marks, *J. Phys. Chem. C*, 2015, **119**, 21018.
39 R. Meyer, L. J. Lewis, S. Prakash and P. Entel, *Phys. Rev. B*, 2003, **68**, 104303.
40 F. Calvo and J. P. K. Doye, *Phys. Rev. B*, 2004, **69**, 125414.
41 D. Y. Sun and X. G. Gong, *J. Phys.: Condens. Matter*, 2002, **14**, 487.
42 M. Tsuji, M. Ogino, R. Matsuo, H. Kumagae, S. Hikino, T. Kim and S.-H. Yoon, *Crystal Growth & Design*, 2009, **10**, 296.
43 M. I. Mendelev, S. Han, D. J. Srolovitz, G. J. Ackland, D. Y. Syn and M. Asta, *Philos. Mag.*, 2003, **83**, 3977.
44 F. Cleri and V. Rosato, *Phys. Rev. B*, 1993, **48**, 22.
45 G. Rossi, R. Ferrando, A. Rapallo, A. Fortunelli, B. C. Curley, L. D. Lloyd and R. L. Johnston, *J. Chem. Phys.*, 2005, **122**, 194309.
46 W. Ma, X. Zhang and K. Takahashi, *J. Phys. D: Appl. Phys.*, 2010, **43**, 465301.
47 V. A. Lubarda, *Mech. Mat.*, 2003, **35**, 53.
48 M.-Y. Ng and Y.-C. Chang, *J. Chem. Phys.*, 2011, **134**, 094116.

View Article Online
DOI: 10.1039/D6CP00043F

The data supporting this article have been included as part of the Supplementary Information. The basic features (numbers of atoms, rounding and prolateness paramters) of deformed nanoparticles, as well as Cartesian coordinates of the initial configurations, are provided as a pdf and a zip file, respectively.